JGR Atmospheres

RESEARCH ARTICLE
10.1029/2018JD029392

Surface Layer Turbulence Parameters Derived From 1-s Wind Observations on the West Florida Shelf

Dennis A. Mayer[1], Jun A. Zhang[2], and Robert H. Weisberg[1]

[1]College of Marine Science, University of South Florida, St. Petersburg, FL, USA, [2]Atlantic Oceanographic and Meteorological Laboratory, Hurricane Research Division, National Oceanographic and Atmospheric Administration, Miami, FL, USA

Key Points:
- Using 1-s wind observations from the West Florida Shelf, turbulence parameters were examined and compared with Kolmogorov similarity theory
- Three events were examined consisting of ensembles of abutting 30-min subsets spanning from 5.5 to 23 hr
- Turbulence parameters were larger than expected; evidence of anisotropy and deviations from similarity suggest improvements are needed in momentum flux algorithms presently operant in numerical models

Correspondence to:
D. A. Mayer and J. A. Zhang,
dmayer@mail.usf.edu;
jun.zhang@noaa.gov

Citation:
Mayer, D. A., Zhang, J. A., & Weisberg, R. H. (2019). Surface layer turbulence parameters derived from 1-s wind observations on the West Florida Shelf. *Journal of Geophysical Research: Atmospheres*, *124*, 1992–2007. https://doi.org/10.1029/2018JD029392

Received 25 JUL 2018
Accepted 23 JAN 2019
Accepted article online 28 JAN 2019
Published online 23 FEB 2019

©2019. American Geophysical Union. All Rights Reserved.

Abstract One-second wind data on the West Florida Shelf were used to examine turbulent scales from large eddies to small eddies in the atmospheric surface layer within a frequency band from 0.02 to 0.3 Hz (periods from ~1 min to ~3 s). Data were collected at two at-sea locations spanning 6.5 months. Three events in three wind ranges were examined in exploring the one-dimensional turbulent power spectra: >14 m/s, wind range I; those between 10 and 14 m/s, wind range II; and those between 5 and 10 m/s, wind range III. Events consisted of ensembles of abutting 30-min subsets spanning 5.5 to 23 hr. The mean vector wind time scale of $T_0 = 30$ min was found to be reasonable for the West Florida Shelf region. The first wind range provided the best results, more or less in line with a Kolmogorov −5/3 power law whose mean vector wind speed over 21 subsets (10.5 hr) was nearly 15 m/s. The one-dimensional turbulent power spectra provided an estimate of the dissipation rate (ε) from which other turbulent quantities could be computed: u^*, τ, and C_d (the frictional velocity, the surface stress, and the drag coefficient, respectively). The salient point here is that these quantities were larger than those from previous observational studies. Where the power law was not operant intrinsic turbulent spatial scales ranged from 1 to 0.1 m and provide evidence of anisotropy for frequencies greater than 0.1 Hz.

Plain Language Summary Wind data sampled at 1 Hz were collected at two at-sea locations on the West Florida Shelf where data common to both moorings span roughly 6.5 months. We showed that a mean vector wind time scale of $T_0 = 30$ min is reasonable for the West Florida Shelf domain. Three wind ranges were examined from which the one-dimensional turbulent power spectra allowed estimates of turbulent parameters crucial in developing momentum flux algorithms used in numerical models of both the atmosphere and the ocean. Turbulence parameters were found to be larger than expected suggesting that improving flux algorithms should be a high priority.

1. Introduction

Local wind forcing on the West Florida Shelf (WFS) is a principal component in forcing the regional coastal ocean circulation together with buoyancy fluxes and interactions with the shelf slope by the Gulf of Mexico Loop Current and its eddies (e.g., He & Weisberg, 2003; Weisberg & He, 2003). The local wind forcing is especially important on the inner shelf that extends out to about the 50-m isobath (e.g., Li & Weisberg, 1999). The background state for the seasonal variability along the shelf is upwelling favorable from fall to spring months (October–April) and downwelling favorable during summer months (June–September; Weisberg et al., 2009). The complexity of the regional shelf circulation requires accurate wind forcing fields for application in numerical models and entails assimilating wind observations to provide an accurate wind forecast. Without accurate wind forecasts the resulting model circulation fields would either be underestimated or overestimated, which would compromise their application in coastal ocean state variable estimation and hence water particle trajectories that impact the environmental distribution of the biosphere and anthropogenic pollutants. Thus, improving our understanding of coupling at the air-sea interface (fluxes of momentum and sensible and latent heat) is the key for improving models of both the atmosphere and the ocean where both vary over a broad range of spatial and temporal scales.

The context for this study of turbulence scales is provided in Mayer et al. (2017) where the wind forcing field was examined in great detail with salient comparisons of National Oceanographic and Atmospheric Administration's (NOAA) National Center for Environmental Prediction reanalysis wind fields (National Center for Environmental Prediction winds) with five University of South Florida Coastal Ocean

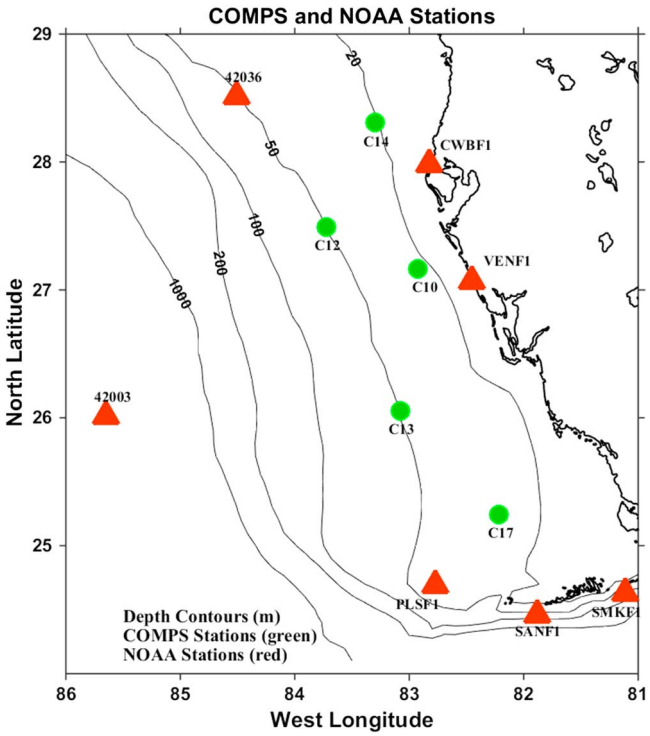

Figure 1. Analysis domain showing NOAA and COMPS stations. NOAA stations are the red triangles and the COMPS stations are the green circles. COMPS = Coastal Ocean Monitoring and Prediction System; NOAA = National Oceanographic and Atmospheric Administration.

Monitoring and Prediction System buoys and seven of NOAA's National Ocean Service and National Weather Service, National Data Buoy Center stations or buoys spanning a 10-year period. These background state mean fields are consistent with those described in Weisberg et al. (2009) and also consistent with the winter and summer fields as given in Liu and Weisberg (2012), where there is a clockwise rotation from winter to summer with much larger amplitudes in winter showing variability dominated by the synoptic weather band (periods from 10 to 3 days). The specific comparisons in Mayer et al. (2017) were designed to provide a rationale for improving the coupling schemes at the air-sea interface and are not relevant in this study. Our objective here relates to examining the highest frequencies of the wind variability available within a subset of the above described wind data set where most of the wind analyses dealt only with hourly winds and are not suitable for looking at coupling schemes.

The analysis domain is provided in Figure 1 and covers an area from 24 to 29°N and from 86 to 81°W. The along-shelf scale of the WFS is approximately 550 km northwestward along the 50-m isobath. The across shelf scale is approximately 150 km from the shoreline to the shelf break. However, the wind data described in Mayer et al. (2017) provides 1-s winds only at two of the moorings (C10 and C13) and only during the years 2013 and 2014. The mooring C10 is 33 km from shore and that at C13 is 122 km from shore. At these distances the data collected here for 309 and 347 days, respectively, qualify as at-sea (>20 km) observations as described by Harper et al. (2009) and are thus in a domain where there are few direct observations over open water. Despite the more than 120-km distance between them, the low-frequency coherence between the winds at C10 and those at C13 is near 0.9 at the 99% significance level as described in Mayer et al. (2017) with essentially no lag within the 6-hr sample intervals and their relative wind angles within 2°.

The frequency bands of interest here extend over a hierarchy of turbulence scales beginning with a production range (injection of energy) with large eddies (integral length scales, Sciremammano, 1979) through a universal equilibrium range that spans an inertial subrange (Kaimal et al., 1972; Lumley, 1967; Miyake et al., 1970), which is a flux of energy through smaller eddies (Taylor microscales, Taylor, 1935), and a dissipation range with the smallest eddies (Kolmogorov length scales, Kolmogrov, 1941). This is based on the Kolmogorov similarity hypothesis where local isotropy (having no preferred direction) of small eddies have evolved from decay of much larger eddies through an equilibrium transfer of energy in the inertial subrange (MacCready, 1962). From Harper et al. (2009), these frequency bands are qualitatively defined in a universal (canonical) spectrum spanning periods from 1,000 hr (42 days) to 0.001 hr (3.6 s). These include the synoptic band, periods from 10 to 3 days, the mesoscale band (periods from a day or so through diurnal, semidiurnal to hourly) and the microscale band (periods from hourly through a few seconds). For applications with data described herein these frequency bands are sketched in Table 1.

What follows is an effort to improve our understanding of coupling at the air-sea interface with an emphasis only on the momentum fluxes considering the limitations of our data set, 1-s winds, and the transfer of energy within the microscale band to the dissipation band from ~0.02 to 0.3 Hz (periods from ~1 min to ~3 s). Our ultimate goal is to improve the model ocean circulation fields and the model atmospheric physical processes as well over the WFS domain. However, our focus here is on the smallest scales not heretofore available with our older wind data sets that were limited to only hourly data. Analysis of the 1-s winds relate directly to the transfer of momentum to the sea surface or the time rate of change of energy per unit mass (dissipation rate, ε), with the latter having units in square meters per cubic second.

Table 1
Frequency Bands

Frequency				
Days	Cpd	Cph	Hz	Period
180	$5.56\ 10^{-3}$	$2.31\ 10^{-4}$	$6.43\ 10^{-8}$	6 months
90	0.0111	$4.63\ 10^{-4}$	$1.29\ 10^{-7}$	3 months seasonal
12	0.0833	$3.47\ 10^{-3}$	$9.65\ 10^{-7}$	begin synoptic
10	0.1	$4.17\ 10^{-3}$	$1.16\ 10^{-6}$	begin synoptic
7	0.143	$5.95\ 10^{-3}$	$1.65\ 10^{-6}$	begin synoptic
4	0.25	0.0104	$2.89\ 10^{-6}$	4 days end synoptic and
3	0.333	0.0139	$3.86\ 10^{-6}$	3 days begin mesoscale
1	1	0.0417	$1.16\ 10^{-5}$	24 hr
0.5	2	0.0833	$2.31\ 10^{-5}$	12 hr
0.0417	24	1	$2.78\ 10^{-4}$	1 hr—spectral gap and
0.0208	48	2	$5.56\ 10^{-4}$	30 min begin microscale
$3.47{\cdot}10^{-3}$	288	12	$3.33\ 10^{-3}$	5 min
$6.94{\cdot}10^{-4}$	1440	60	0.0167	1 min
$5.79{\cdot}10^{-5}$	$1.73\ 10^{4}$	720	0.2	5 s begin dissipation
$3.47{\cdot}10^{-5}$	$2.88\ 10^{4}$	1200	0.33	3 s

Note. The values in this table were pieced together from the descriptions of a canonical wind spectrum from Harper et al. (2009) and the discussion of the different frequency bands from Mikkelsen et al. (2017) and also from Mayer et al. (2017), which provided the context for this work.

2. Data

To provide a low-frequency context for the 1-s wind analyses the observations were 40-hr low-pass filtered (using a fifth-order Butterworth filter, 6 dB down at 39 hr and 20 dB down at 32 hr) and resampled every 8 hr. The results are plotted in Figure 2.

This separates the higher frequencies—the focus of our present analysis—from the lower frequencies with periods longer than 2 days that describe regional wind variability from seasonal to synoptic (associated with the passage of frontal systems). Note the diminished wind speeds during summer usually beginning in June and ending in September.

The 1-s wind observations were obtained using a 1405-PK Gillwindsonic anemometer. The instrument output does not include the vertical wind component but provides the horizontal velocity directly in terms of the eastward and northward components every second and so this might be considered an instantaneous measurement. The wind coordinates are internally hard wired. The magnetic declination correction is added to the raw data as part of our quality control procedures that also account for outliers and other issues. The instrument is located at 3.1 m above the sea surface at the top of the buoy tower, which essentially eliminates any flow distortion from the buoy structure. The 1-s sample rate theoretically allows an analysis up to the Nyquist frequency (0.5 Hz), but for reasons outlined below the highest frequencies are limited to no more than 0.3 Hz. The time series in Figure 2 are a subset of the complete record described in Mayer et al. (2017) along with details of the buoy moorings. For the subset of 1-s winds there are 309 days from 10 September 2013 to 15 July 2014 at C10 and 347 days from 29 December 2013 to 11 December 2014 at C13. All of the wind observations were referenced to 10-m height using a neutral drag coefficient following the method of Large and Pond (1981), the same as in Mayer et al. (2017).

The background state for the atmosphere was derived from average conditions at C10, air density (1.19 kg/m^3), temperature (22.8 °C), pressure (1,017 hPa), and relative humidity (78%). The data include all available data at C10 from 19 August 1998 to 10 September 2013, well over 10 years. These conditions were relevant to the derivation of wind stress described in Mayer et al. (2017).

3. Analysis

3.1. Overview

The analyses that follow consider the cascade of turbulence scales from large eddies to small eddies focusing on a frequency range between 0.02 and 0.3 Hz (periods from ~1 min to ~3 s), although the lower frequencies

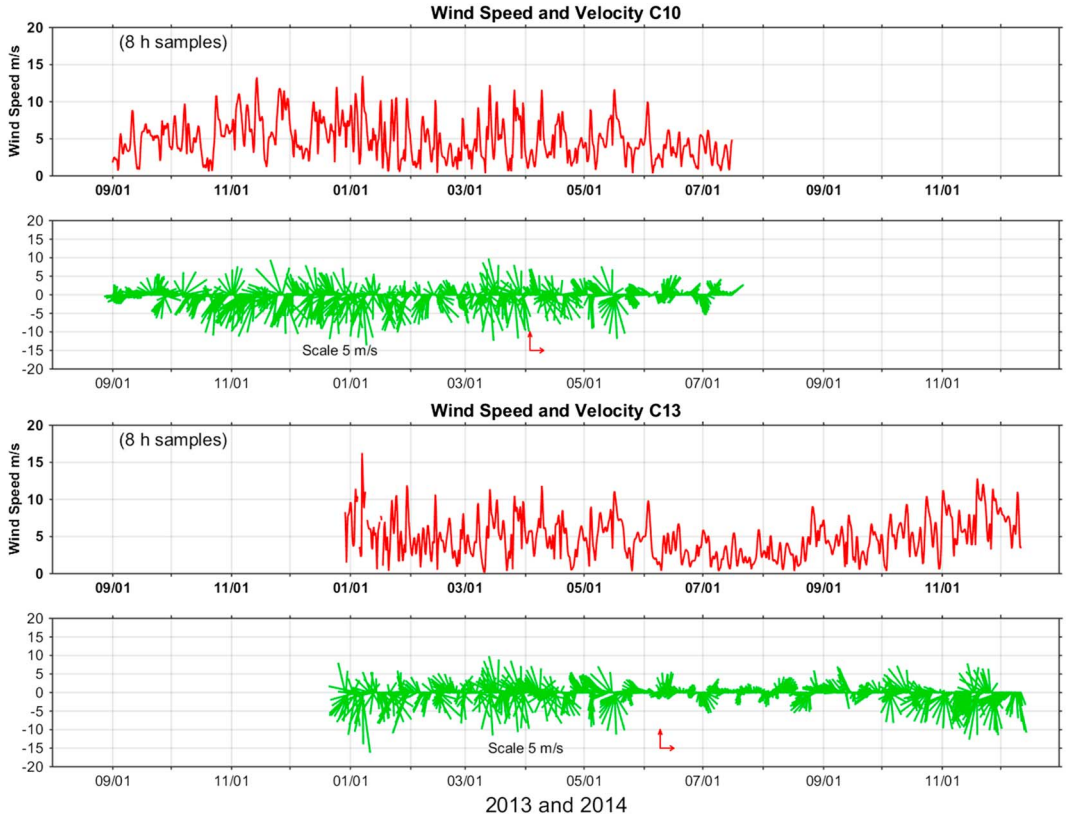

Figure 2. Comparison of 40-hr low-pass-filtered Coastal Ocean Monitoring and Prediction System observations at C10 and C13.

from 10^{-7} to 10^{-3} Hz (periods from 116 days to ~17 min) are discussed for completeness. All observations fall well within the atmospheric surface layer of order 100 m (Kaimal & Finnigan, 1994). The higher end of the low frequencies (periods from 1 hr to 30 min) falls within a spectral gap (Harper et al., 2009), which is critical in organizing the data into sequences of mean wind time scales ($T_0 = 30$ min) where the observations are more or less quasi-stationary and from which velocity and spatial scales of turbulence can be estimated. The context here examines turbulence scales against Kolmogorov's similarity hypothesis, which provides a physical basis for describing what follows, particularly if there is evidence of anisotropy.

The limitations of our analyses relate to both the sample rate of 1 Hz and the absence of vertical velocity observations. Accurate measurements of turbulence require a sample rate greater than 5 Hz (Harper et al., 2009). Despite this, substantive results can be obtained with the lower sample rate as described in Zhang et al. (2011). As will emerge any frequencies exceeding 0.3 Hz are seriously compromised by either buoy mooring motions or energy that is aliased from the very high frequencies, so these frequencies will be ignored. However, not having direct measurements of the vertical component of velocity is an issue that can be avoided by utilizing the −5/3 power law, if applicable for the one-dimensional turbulent power spectra. This is described by MacCready, (1962), Large and Pond (1981), Yelland and Taylor (1996), and more recently Zhang et al. (2009, 2011) where the spectra can be derived with either a frequency or wave number rendition. The wave number version from MacCready (1962) is $\phi(k) = C_k < \varepsilon >^{2/3} k^{-5/3}$. Units are in cubic meters per square second, k is the wave number, C_k is the Kolmogorov constant and is equal to 0.5, an approximation used by Zhang (2010) and is supported by experimental results from Sreenivasan (1995), and ε is the dissipation rate described above (m^2/s^3). This is the source but, as it relates to the frequency domain, is equivalently $\phi(f) = C_k < \varepsilon' >^{2/3} f^{-5/3}$ with units square meters per second. The difference here is that ε is scaled with $\varepsilon' = \varepsilon\,(U_0/2\pi)$ and the quantity U_0 is the along mean vector wind speed. For the dissipation rate the frequency rendition as derived by Zhang et al. (2009) is $\varepsilon = C_k^{-3/2}\,(2\pi f/U_0)(f\phi(f))^{3/2}$. The quantity $\phi(f)$ is the one-dimensional turbulent power spectra (spectral density, $m^2/s^2/\Delta f$) with Δf as the resolution

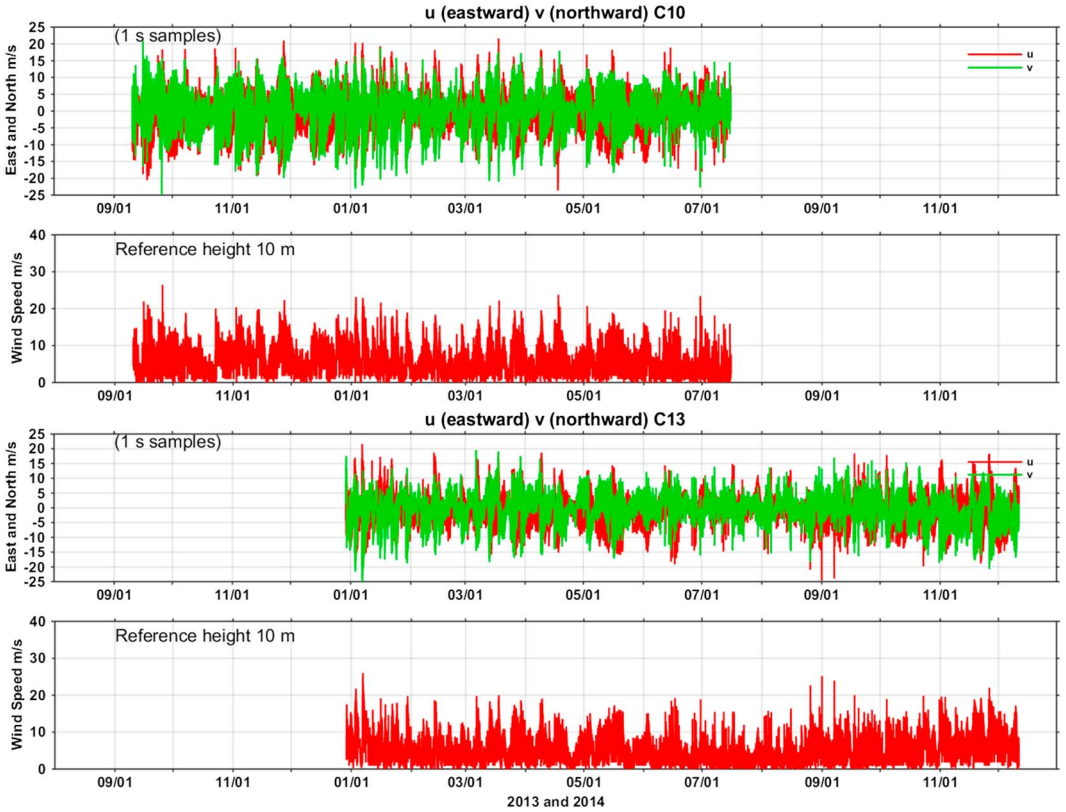

Figure 3. One-second winds from Coastal Ocean Monitoring and Prediction System observations at C10 and C13.

frequency (c/s). For completeness the wave number version is $\varepsilon = C_k^{-3/2}\,(k)\,(k\,\phi(k))^{3/2}$ with the wave number (k) equivalent to $2\pi f/U_0$. Alternatively, the spectra can also be derived as $k\,\phi(k) = C_k < \varepsilon >^{2/3} k^{-2/3}$ (a 2/3 power law) in terms of the wave number or as $f\,\phi(f) = C_k < \varepsilon' >^{2/3} f^{-2/3}$ in terms of the frequency (both with units in square meters per square second). For our purposes all estimates of spectra and dissipation rate will be computed in terms of frequency.

As a prelude to the spectral analyses that follow the complete 1-s winds are provided in Figure 3. Most large wind excursions are a consequence of winter frontal passages. The maximum observed 1-s wind speeds are 26.5 and 26.0 m/s at C10 and C13, respectively, and complement the low-frequency renderings in Figure 2. Also with respect to gusts, the maximum 3-s average within each 30-min subset is a 3-s gust, and for all abutting subsets spanning all the data, the maximum gust is 25.0 m/s for both C10 and C13, which is very close to the maximum 1-s wind speeds. Further the mean vector wind over an averaging period of 30 min ($T_0 = 30$ min and 1,800 s) does not exceed 16.7 m/s at C10 and 16.4 m/s at C13. So throughout the observational time period, there are no events—events that consist of ensembles of abutting 30-min subsets spanning 5.5 to 23 hr—that the mean vector wind exceeds the threshold of tropical storm wind speed (17.4 m/s).

Once the spectra are examined, it will become clear that the mean vector wind time scale of 30 min is a good choice in this WFS region. In other words, this time scale within the spectral gap allows a reliable estimate of quasi-stationary statistics. To this end, the composite spectral density, $\phi(f)$, for the complete data set at C10 and C13 are shown in Figure 4. These are only of wind speed and have not been separated into along and across the mean vector wind, which for the entire record from both moorings are 1.914 m/s along a bearing of −126.5° T (true, corrected for magnetic declination) for C10 and 1.931 m/s along a bearing of −116.4° T for C13.

The other version of spectra using $f\,\phi(f)$ is in Figure 5. Note what appears to be anomalously large energy beyond 0.3 Hz for both spectral versions. This does not obtain in Zhang et al. (2011) where their 1-s spectra did not show this increase beyond 0.3 Hz. We can only speculate here, as their observations were obtained from aircraft, which suggests that buoy motion might be responsible. Another possibility is that aliasing

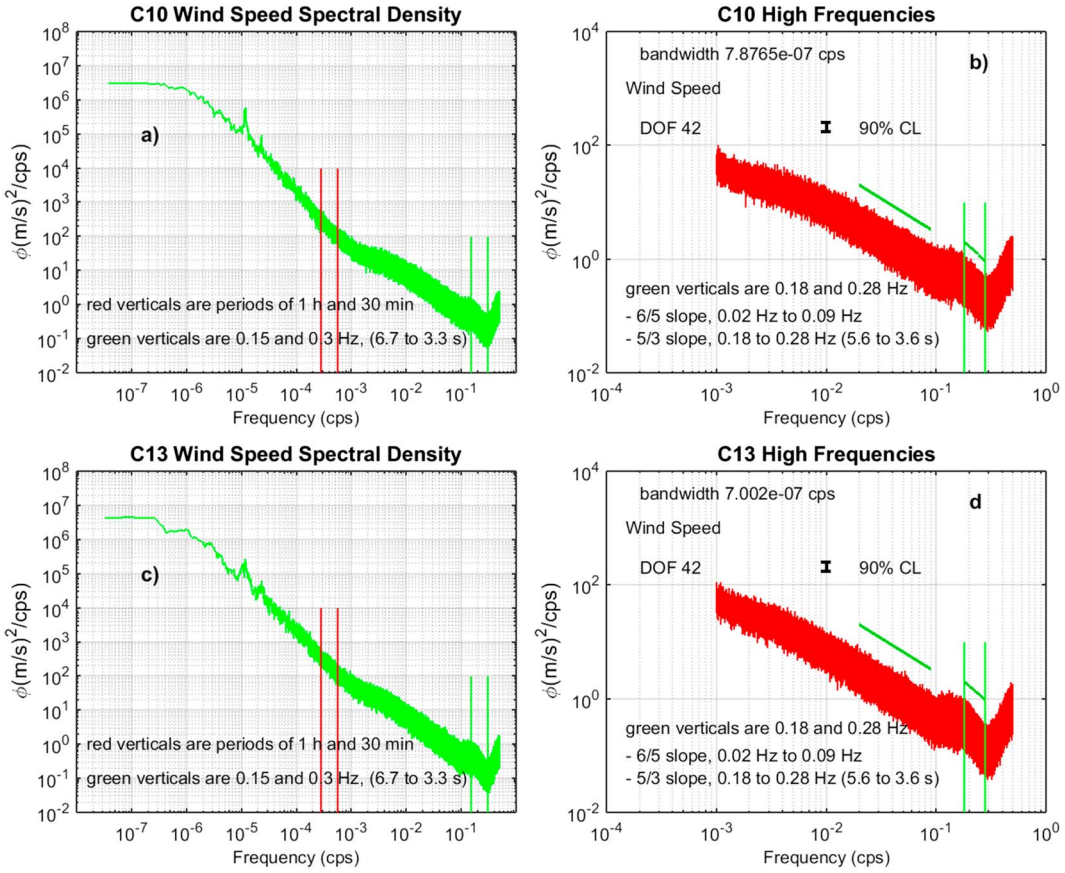

Figure 4. Composite spectra $\phi(f)$ of wind speed derived from 1-s winds from Coastal Ocean Monitoring and Prediction System observations at C10 and C13. Slopes are also indicated. (a) Full spectrum for C10 showing the spectral gap between periods of 1 hr and 30 min (red verticals). Green verticals denote the band between 0.15 and 0.3 Hz. (b) High frequencies for C10 but showing the 90% CL and the two slopes between 0.02 to 0.09 Hz (−6/5) and that between 0.18 and 0.28 Hz (−5/3). (c) Same as in (a) but for C13. (d) Same as in (b) except for C13. CL = confidence limits; DOF = degree of freedom.

from much higher-frequency turbulence that cannot be resolved with a 1-s sample rate could also be responsible. In any case, the spectra with frequencies above 0.3 Hz will be ignored.

With regard to the spectral gap, Figure 5 shows the region where the gap is near a period of 30 min (~5.6×10^{-4} Hz) for both moorings. The actual minimum is closer to 10^{-3} Hz (~17 min). This is well within what is described by Harper et al. (2009) regarding the spectral energy gap—periods between 3 hr up to about 20 min between the mesoscale and the microscale—where under many different conditions over both land and sea the energy distribution is quite flat in this frequency range and there is much less variability. The result is that the mean is largely independent of the length of record and averaging over such periods is consistent with the desire to have statistically stationary samples. We chose to use the time scale of T_0 = 30 min rather than a period of ~17 min because the latter would limit the number of observations for each subset in computing the mean vector wind speed and direction and provide better resolution for the spectral analyses that follow. Each subset provides 1,800 one-second samples and good resolution in the frequency domain where assumptions about quasi-stationarity seem reasonable. The spectral gap is also nominally described by Mikkelsen et al. (2017) lying between 10^{-4} and 10^{-3} Hz where the spectral energy is quite low and the boundary layer turbulence is weak in this region. Above these frequencies, the turbulence is more intense. With regard to the universal (canonical) spectrum, the plot in Figure 5 is very much in line with that described in Harper et al. (2009) and by Mikkelsen et al. (2017) with some differences. Previous studies on turbulent flux calculations using buoy data also used a time scale of 30 min for each flux run (e.g., Donelan et al., 1997; Drennan et al., 1999; Fairall et al., 1996; Katsaros et al., 1993; Potter et al., 2015; Smith, 1980).

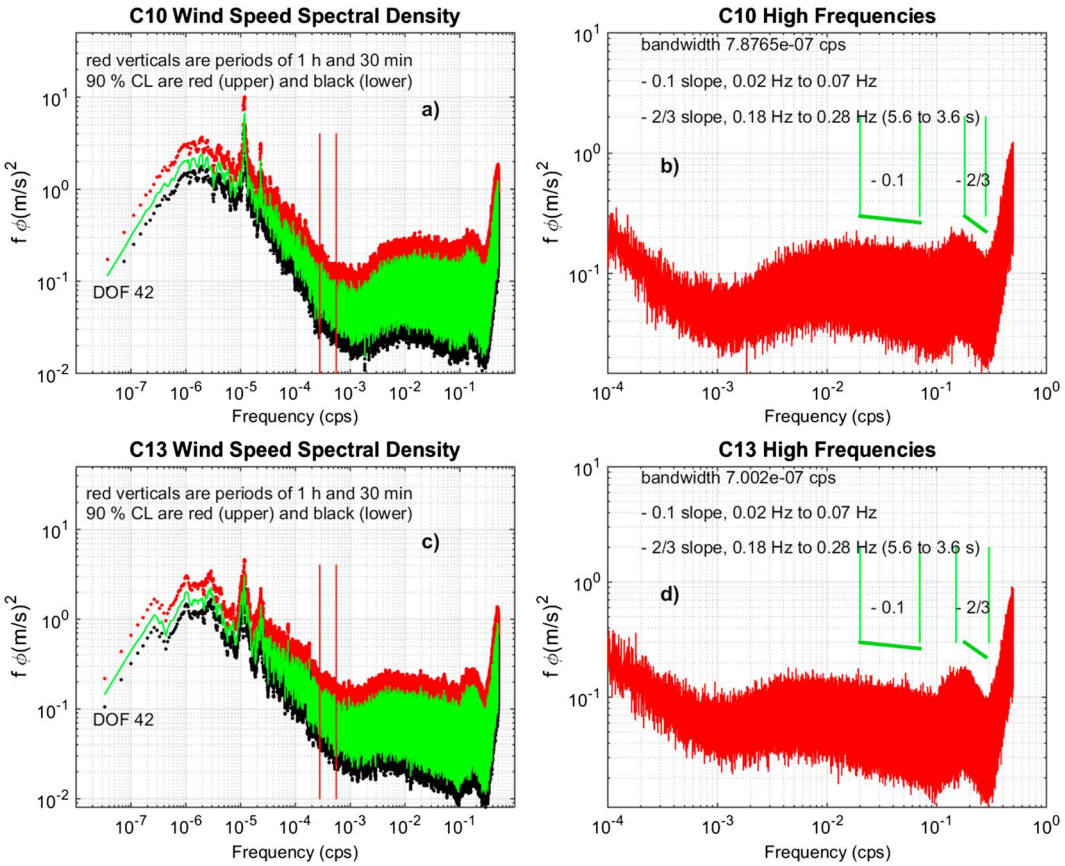

Figure 5. Composite spectra $f\,\phi(f)$ of wind speed derived from 1-s winds; 90% CL are indicated in (a) and (c). Slopes are indicated in (b) and (d). (a) Full spectrum for C10 showing the spectral gap between periods of 1 hr and 30 min (red verticals). (b) High frequencies for C10 but showing the two slopes between 0.02 to 0.07 Hz (−0.1) and that between 0.18 and 0.28 Hz (−2/3). (c) Same as in (a) but for C13. (d) Same as in (b) except for C13. CL = confidence limits; DOF = degree of freedom.

One salient point in the lower frequencies is the robust nature of the diurnal peak. This along with the semi-diurnal peak is a consequence of the sea breeze. Both bracket a band of 21 frequencies whose periods span 24.9 to 23.2 hr for the diurnal band and 12.2 to 11.8 hr for the semidiurnal band. Note that that these effects degrade seaward as the diurnal energy is significantly less at C13 than at C10 because C13 is more than 100 km farther from shore than C10. Moreover, Mikkelsen et al. (2017) provide a very thorough analysis at several heights over land and characterizes turbulence data for frequencies whose periods are less than about 10 min with the spectra for frequencies above about 0.02 Hz varying according to a −2/3 power law (Figure 5) or a −5/3 power law as in Figure 4. However, for our data this is clearly not the case between 0.02 and 0.07 Hz. They also suggest that Taylor's frozen turbulence hypothesis is valid for frequencies above the diurnal band spanning both the mesoscale and microscale range and becomes more accurate with increasing frequency. They also posit that the shear production range of turbulence within an eddy surface layer is extant in the frequency band between 10^{-3} and 10^{-1} Hz. For completeness the eddy surface layer is nominally one third the height of the surface layer, which is roughly one tenth the height of the atmospheric boundary layer (~1 km).

Acknowledging that the above spectra are not one-dimensional but are of the wind speed, a −5/3 and −2/3 slopes have been plotted in Figures 4 and 5, respectively, in the frequency range from 0.18 to 0.28 Hz (marginally in the dissipation range). The slopes seem to match here at C10 but at C13 the slope appears more severe and suggests a more complicated physics than that advanced by Zhang (2010). The slopes in the frequency range 0.02 to 0.07 Hz are slightly shallower than those between 0.18 and 0.28 Hz in Figure 4 but are essentially the same for both C10 and C13 (~−6/5) and much shallower in Figure 5, nearly flat.

Table 2
Mean Vector Wind Statistics for Three Events in Three Wind Ranges

Wind range	Mooring	Date	Time span (hr)	Mean wind (m/s) ±σ	Direction (° true) ±σ
I	C10	1/07/2014	5.5	14.97 ± 0.49	162.9 ± 2
II	C10	5/16/2014	9.5	11.44 ± 0.45	175.9 ± 10
III	C10	5/04/2014	23	7.49 ± 0.46	172.2 ± 9
I	C13	1/07/2014	10.5	14.97 ± 0.52	167.2 ± 4
II	C13	5/16/2014	9	11.65 ± 0.43	−175.1 ± 2
III	C13	5/04/2014	22	7.07 ± 0.96	−178.5 ± 9

Note. Wind ranges: I > 14 m/s, II = 10 to 14 m/s, and III = 5 to 10 m/s.

Our focus regards frequencies greater than 0.02 up to 0.3 Hz, which spans the higher frequencies of the shear production range through the lower end of the dissipation range assuming that an inertial subrange exists where the shear production subrange at lower wave numbers cascades through an inertial subrange, which is balanced by the dissipation rate ε. This conceptual similarity model requires stationary and isotropic turbulence, which may deviate from this picture as described by Mikkelsen et al. (2017). However, these assumptions have been used in other situations as in Zhang et al. (2011) where they assert that reasonable estimates of turbulent quantities can be derived by real observational data, albeit not near the surface as their observations were obtained aloft in an aircraft. Whether or not local isotropy and Kolmogorov's similarity hypothesis applies is a question that needs to be addressed where there are deviations as provided in the spectral plots in Figures 4 and 5.

3.2. Three Wind Ranges

What follows is an attempt to explore the one-dimensional turbulent power spectra described above. We will look at the statistics-variability of the mean vector wind using the (T_0 = 30 min) time scale. This provides a set of independent subsets as described below by virtue of an integral (independence) time scale and appears to be a good choice for the regional variability on the WFS as shown above (Figure 5). Our approach will identify several events for each mooring in three wind ranges: those exceeding 14 m/s, wind range I; those between 10 and 14 m/s; wind range II; and those between 5 and 10 m/s, wind range III. These are approximately a Beaufort range of near gale, fresh-to-strong breeze, and moderate breeze, respectively. As will emerge each event is characterized by an ensemble of T_0 (30 min) abutting subsets that span the event and each subset is one member of the ensemble. All relate to synoptic spring and winter frontal passages confined to the data that overlap in time, approximately 6.5 months. The time spanning each event ranges between 5.5 and 23 hr. Mean vector wind speed and directions were computed for each subset within the ensemble comprising a given event and are more or less synoptic, with a caveat that allows for a delay of frontal movement between C10 and C13 from 1 to 6 hr. The highest wind range (I) exhibits the least delay and is almost synoptic with the largest delay at the lowest wind range (III). The data in Table 2 provide the mean vector wind statistics for each event along with the dates and duration of each.

For the ensemble means in Table 2, the values for σ were used in computing ϵ (standard error) = $\sigma/\sqrt{\eta}$, where η is the number of degrees of freedom (DOFs), which is defined as $\eta = T_0/t\mathrm{I}$. The quantity tI is the integral (independence) time scale defined as in Sciremammano (1979). This integral scale is also consistent with that described in Yu et al. (2008). For the 1-s winds in each subset, this scale is of order from 1 to 3 min based on the large lag standard error = $1/\sqrt{\eta}$. For the worst case of tI = 3 min (180 s), DOF > 10 for each subset. This together with a minimum event time span of 5.5 hr (11 subsets of 30 min each) provides values for DOF > 110. The standard error (ϵ) then reduces the values of σ by at least one tenth and is a strong argument for advancing a context of quasi-stationarity for the ensemble of subsets within each event.

To visualize the nature of this variability a scatter plot of one member of the ensemble in wind range I for both C10 and C13 is provided in Figure 6 before the data were detrended otherwise all the values would be clustered about the origin. Although this is only one subset of a 5.5-hr event, the balance of the other ensemble members are essentially equivalent. This applies to the other two wind ranges as well except for smaller vector mean winds thus rendering unnecessary any more plots. Note here that the turbulence intensity (TI) is provided as TIA, intensity along the mean vector wind, and TIX, intensity across the mean vector

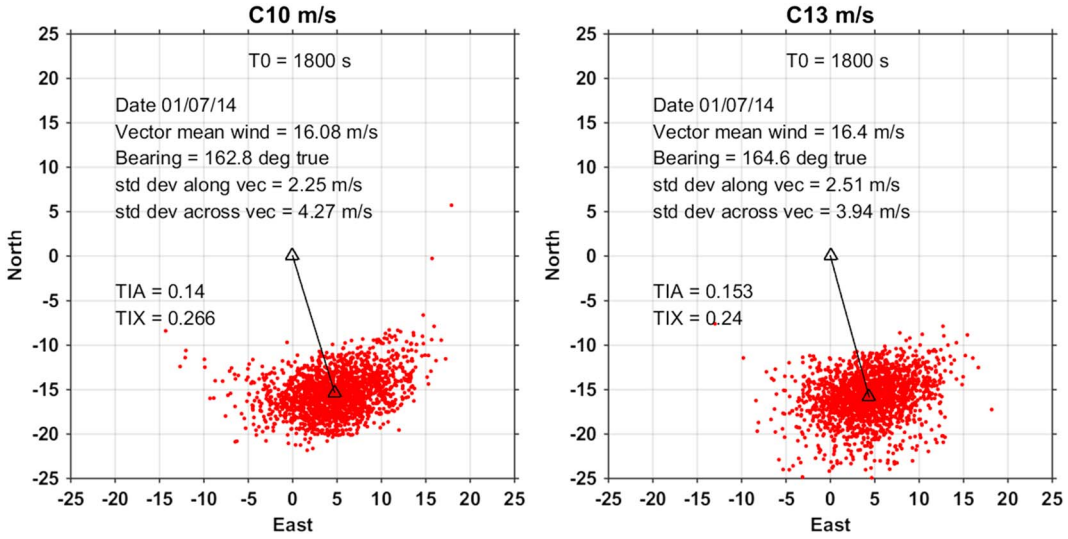

Figure 6. A representative 30-min subset during a wind range I event over 5.5 hr on 7 January 2014 at C10 and C13. Each dot is one observation of a 1,800-s sample. TIA and TIX are TI (turbulence intensity) along and across the mean vector wind, respectively. Here TI is defined as TI = σ/U_0, where σ is the standard deviation along and across the mean vector wind. Speeds exceed 16 m/s along a bearing of 163° to 165° T.

wind. The values are based on detrended data in the along and across wind coordinate system as TI = σ/U_0, where σ is the standard deviation along and across the mean vector wind speed and U_0 is the along mean vector wind speed. The salient point here is that the TIA values are roughly half that of the TIX values.

3.3. Composite Spectra

The composite one-dimensional turbulent power spectra, $\phi(f)$ of detrended data for the three wind ranges described above, are provided in Figures 7–9 for wind ranges I–III, respectively. To be clear, as described above, an ensemble of 30-min subsets define an event. Spectra for each subset were averaged over all member subsets. So in wind range I, for example, in Figure 7, there are 11 subsets of spectra for C10 and 21 subsets for C13. Our goal here is to better understand how momentum flux is transferred to the sea surface in the context of Kolmogorov's similarity hypotheses requiring isotropy. Where there are events that deviate from this paradigm, we can still compute the intrinsic velocity and spatial scales directly from the turbulence spectra providing intelligence on processes that may be anisotropic.

Although the spectral plots span frequencies from 0.01 to 0.3 Hz, it seems that the most salient results could be derived from frequencies greater than 0.1 Hz as in Zhang et al. (2011), which is the lower end of the dissipation range and also assuming a priori that an inertial subrange exists. This would be consistent with Kolmogorov's hypotheses where eddy motion is assumed to be independent of viscosity and determined entirely by the rate of energy transfer, which is equal to the rate of energy dissipation ε at higher frequencies.

So there are two dimensions to what follows. The first relates to calculations of the dissipation rate and related quantities, unfortunately in only a narrow frequency band where the −5/3 law seems to be more or less valid. The second relates to the intrinsic turbulent velocity and spatial scales that can be derived directly from the spectra at other frequencies. These are the scales of turbulent fluctuations but not necessarily the eddy scales.

From Figures 7 and 8, between 0.15 and 0.25 Hz, the slopes for wind range I are −4/3 and −5/3 for C10 and C13 and for wind range II they are −4.4/3 and −6/3, respectively. So these slopes range from −4/3 to −6/3 and bracket a −5/3 slope. Arguably, these are not exactly −5/3 but are close enough to derive the dissipation rate $\varepsilon = C_k^{-3/2}\,(2\pi f/U_0)\,(f\phi(f))^{3/2}$ where the quantity $\phi(f)$ is the computed one-dimensional turbulent power spectra. So with ε the frictional velocity $u^* = (\varepsilon\,\kappa\,z)^{1/3}$ follows where κ is the Von Karman constant equal to 0.4 and z is the measurement height (10 m). With u^* you can compute the momentum flux $\tau = \rho\,u^{*\,2}$ (Pa or N/m^2) and then the drag coefficient $C_d = (u^*/U_0)^2$. Of note, estimating the momentum flux using the dissipation rate is based on the assumption that the shear production balances the dissipation rate in the

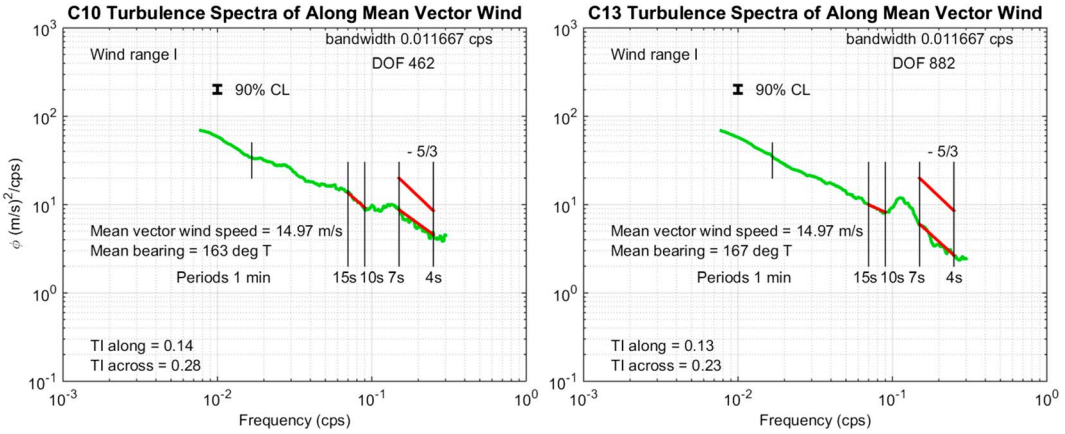

Figure 7. Composite one-dimensional spectra $\phi(f)$ of along mean vector wind speed derived from 1-s winds for C10 (left panel) and C13 (right panel) in wind range I from 0.01 to 0.3 Hz; 90% CL are indicated. This is a composite of 11 T_0 = 30-min subsets for C10 and 21 subsets for C13 occurring on 7 January 2014. The −5/3 slopes are shown in the frequency band from 0.15 to 0.25 Hz. The vertical lines denote frequencies of 1/60, 0.07, 0.09, 0.15, and 0.25 Hz. Actual slopes are ~−5/3 Hz between the first two vertical bars and ~−4/3 Hz for the second two vertical bars for C10. For C13 these are ~−2.4/3 and ~−5/3 Hz, respectively. DOF > 460. CL = confidence limits; DOF = degree of freedom.

turbulent kinetic energy budget in the inertial subrange, the so-called *inertial dissipation method* that has been widely used in air-sea flux studies (e.g., Drennan et al., 2005; Dupuis et al., 1997; Edson et al., 1991; Fairall & Larsen, 1986; Large & Pond, 1981; Taylor & Yelland, 2001; Yelland et al., 1994, 1998; Yelland & Taylor, 1996). Here we use $\rho = 1.19$ kg/m^3 as described above for the atmospheric background state with these calculations confined to the frequency range from 0.15 and 0.25 Hz for only wind ranges I and II as the −5/3 power law does not apply in wind range III.

3.4. Dissipation Rate (ε) and Other Quantities

From Figures 7 and 8 for wind ranges I and II we can estimate the dissipation rate ε and the other quantities described above: u^*, τ, and C_d. Their statistics are summarized in Table 3 for the first two wind ranges over the frequency range from 0.15 and 0.25 Hz. Quantities are mean (μ), standard deviation (σ), maximum (max), and minimum (min).

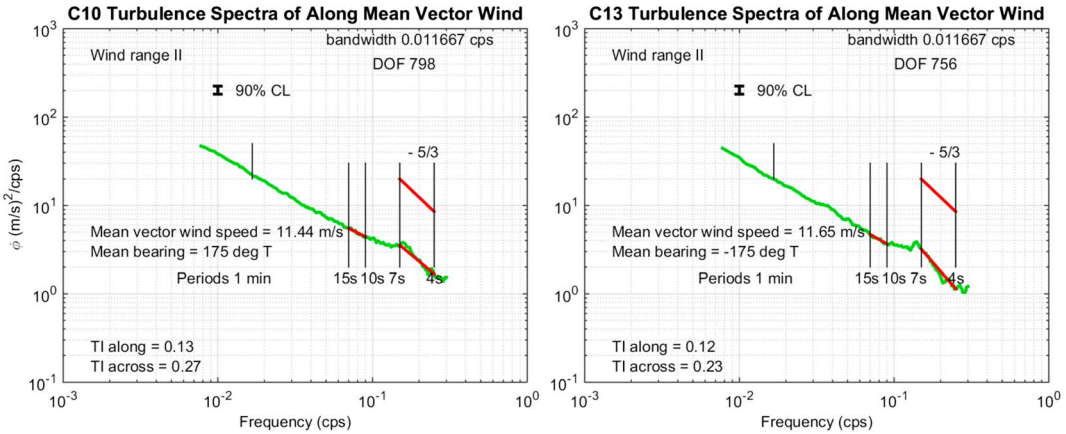

Figure 8. Composite one-dimensional spectra $\phi(f)$ of along mean vector wind speed derived from 1-s winds for C10 (left panel) and C13 (right panel) in wind range II from 0.01 to 0.3 Hz; 90% CL are indicated. This is a composite of 19 T_0 = 30-min subsets for C10 and 18 subsets for C13 occurring on 16 May 2014. The −5/3 slopes are shown in the frequency band from 0.15 to 0.25 Hz. The vertical lines denote frequencies of 1/60, 0.07, 0.09, 0.15, and 0.25 Hz. Actual slopes are ~−2.6/3 Hz between the first two vertical bars and ~−4.4/3 Hz for the second two vertical bars for C10. For C13 these are ~−3/3 and ~−6/3 Hz, respectively. DOF > 750. CL = confidence limits; DOF = degree of freedom.

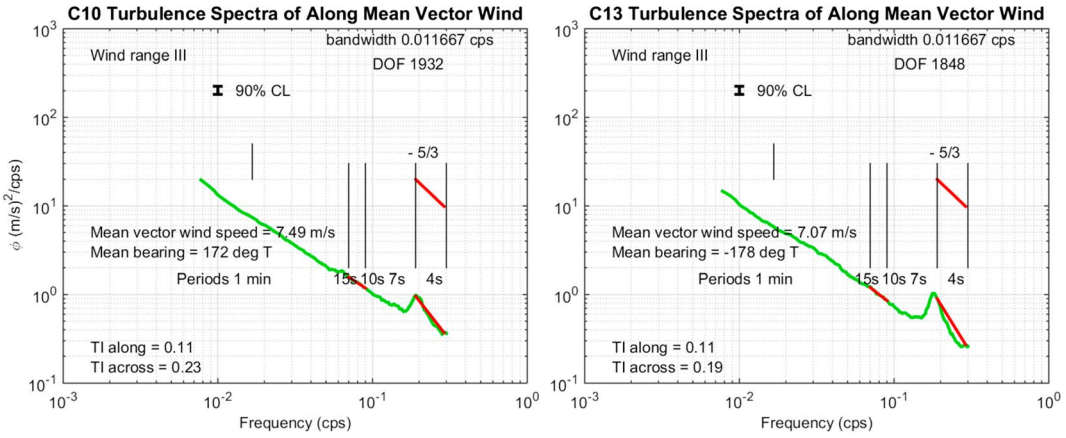

Figure 9. Composite one-dimensional spectra $\phi(f)$ of along mean vector wind speed derived from 1-s winds for C10 (left panel) and C13 (right panel) in wind range III from 0.01 to 0.3 Hz; 90% CL are indicated. This is a composite of 46 $T_0 = 30$-min subsets for C10 and 44 subsets for C13 occurring on 4 May 2014. The −5/3 slopes are shown in the frequency band from 0.19 to 0.29 Hz. The vertical lines denote frequencies of 1/60, 0.07, 0.09, 0.19, and 0.29 Hz. Actual slopes are ~−3.5/3 Hz between the first two vertical bars and ~−6.7/3 Hz for the second two vertical bars for C10. For C13 these are ~−4.1/3 and ~−10.6/3 Hz, respectively. DOF > 1,800. CL = confidence limits; DOF = degree of freedom.

Although these statistics are over a very narrow frequency band by necessity considering the 1-Hz sampling interval, the slopes from Figures 7 and 8 are very close to −5/3 especially for C13 in wind range I and nearly so for C10 in wind range II. Moreover, Zhang et al. (2011) point out that "1 Hz data cannot ordinarily capture the whole spectrum of turbulent energy." Nevertheless, "this limitation notwithstanding we believe that the 1 Hz data have their merit for estimating turbulence parameters." Also, the narrow frequency band considered here is near the higher frequencies of the shear production range and extends through the lower end of the dissipation range. Hence, Table 3 delineates the turbulence parameters derived from the spectrum $\phi(f)$, and assuming that Kolmogorov's hypothesis is valid for these cases, then $\phi(f) = C_k < \varepsilon' >^{2/3} f^{-5/3}$ allows for the calculation of the other three turbulence quantities (u^*, τ, and C_d).

For these two events, the dissipation rates and drag coefficients are considerably larger than that reported by Zhang (2010) and Zhang et al. (2011) by as much as 2 to 3 times for the drag coefficients and up to 10 times for the dissipation rates for comparable mean vector wind speeds. This is probably because their observations were taken at altitudes above the surface layer (>100 m), while our data were collected within the surface layer (~10 m). On the other hand, our estimates of dissipation rate are comparable to those based

Table 3
Statistics for ε, u, τ, and C_d Over Frequencies From 0.15 to 0.25 Hz*

Wind range	I		II	
Mooring	C10	C13	C10	C13
U_0 (m/s)	14.97	14.97	11.44	11.65
ε (cm^2/s^3)				
μ, σ	2,873, 423	1,453, 169	1,024, 96	618, 83
max, min	4,001, 2,105	1,817, 1,079	1,203, 795	770, 446
u^*(m/s)				
μ, σ	1.045, 0.051	0.833, 0.033	0.742, 0.023	0.626, 0.028
max, min	1.170, 0.944	0.899, 0.756	0.784, 0.683	0.675, 0.563
τ (N/m^2)				
μ, σ	1.303, 0.127	0.827, 0.065	0.656, 0.041	0.468, 0.042
max, min	1.628, 1.061	0.962, 0.680	0.731, 0.555	0.543, 0.377
$C_d \times 10^{-3}$				
μ, σ	4.88, 0.48	3.10, 0.25	4.21, 0.26	2.89, 0.26
max, min	6.10, 3.98	3.61, 2.55	4.69, 3.56	3.36, 2.33

Note. μ, σ are mean and standard deviation, respectively. All quantities derived in this table stems from the −5/3 power law.

Table 4
Statistics for L(f) and U(f) Over Frequencies From 0.15 to 0.25 Hz for Wind Ranges I and II and Frequencies From 0.19 to 0.29 Hz for Wind Range III

Wind range	I		II		III	
Mooring	C10	C13	C10	C13	C10	C13
U_0 (m/s)	14.97	14.97	11.44	11.65	7.49	7.07
L_u (cm)						
μ	41.5	33.4	27.3	23.3	10.8	9.06
σ	10	9.3	7.8	7.3	3.2	3
L_v (cm)						
μ	69.9	59	51	47.6	21.5	16.9
σ	16.5	9.9	11.6	11	3.5	2.7
U_u (cm/s)						
μ	8.02	6.42	5.24	4.46	2.49	2.09
σ	0.73	0.81	0.72	0.71	0.42	0.42
U_v (cm/s)						
μ	13.54	11.51	9.87	9.22	5.08	3.98
σ	1.23	0.3	0.76	0.76	0.27	0.19

Note. Subscripts u and v refer to along and across the mean vector wind, respectively; μ, σ are mean and standard deviation, respectively.

on buoy and ships' observations in the atmospheric surface layer in low-wind conditions (e.g., Donelan et al., 1997; Dupuis et al., 1997; Yelland et al., 1998; Yelland & Taylor, 1996). However, the fidelity to the −5/3 power law is well represented for C13 in wind range I, and hence, we are confident that the values of a little over 1,400 cm^2/s^3 for ε and 3.1×10^{-3} for C_d are well rendered. Here also and unique to C13 is a well-defined peak near 0.11 Hz well before the start of the −5/3 slope beginning at 0.15 Hz. Note also that the values for TI are also provided and are consistent with those in Figure 6, which is just one subset of the 5.5-hr event.

For completeness we revisited the data for C13 in wind range I where the −5/3 power law appears to be operant for the along mean vector wind spectrum given in Figure 7. Using the same atmospheric background state described above, we computed the bulk statistics for this event that consisted of 21 subsets of 1,800 s each (37,800 observations) using the 1-s variable drag coefficients (Cd) as described in Large and Pond (1981). This provided a direct route to compute u^*, ε, and τ. The results yielded a drag coefficient of $C_d = 1.47 \times 10^{-3}$ and values for $u^* = 0.574$ m/s, $\varepsilon = 476$ cm^2/s^3, and $\tau = 0.39$ N/m^2, which are roughly one half, two thirds, one third, and one half, respectively, of those in Table 3. So whether or not this particular event with mean vector wind speeds of 14.97 ± 0.52 m/s is consistent with Kolmogorov's similarity hypotheses, is a question that needs to be addressed, especially where bulk estimates of turbulence parameters underestimate the statistics in Table 3 by a factor of approximately 2 or more.

3.5. Velocity and Spatial Scales

Although there is a large range of frequencies that are not amenable to a −5/3 power law, we can still compute the intrinsic turbulent velocity and spatial scales for all three wind ranges derived directly from $\phi(f)$ with $U(f) = (2\Delta f\, \phi(f))^{1/2}$ where U(f) and $\phi(f)$ are either along or across mean vector wind components and spectra, respectively. The intrinsic spatial scales follow with $L(f) = U(f)/f$. The base length scales can also be derived simply with $L_b = U_0/f$.

The intrinsic turbulent velocity and spatial scale statistics for all three wind ranges are summarized in Table 4 and plotted in Figures 10–12. As in Figures 7–9, the velocity and spatial scales span frequencies from a little higher than 0.01 up to 0.3 Hz. The base length scales (L_b) vary from 1,220 to 50 m for wind range I, 930 to 40 m for wind range II, and 600 to 25 m for wind range III. With regard to the intrinsic scales L(f) and U(f),

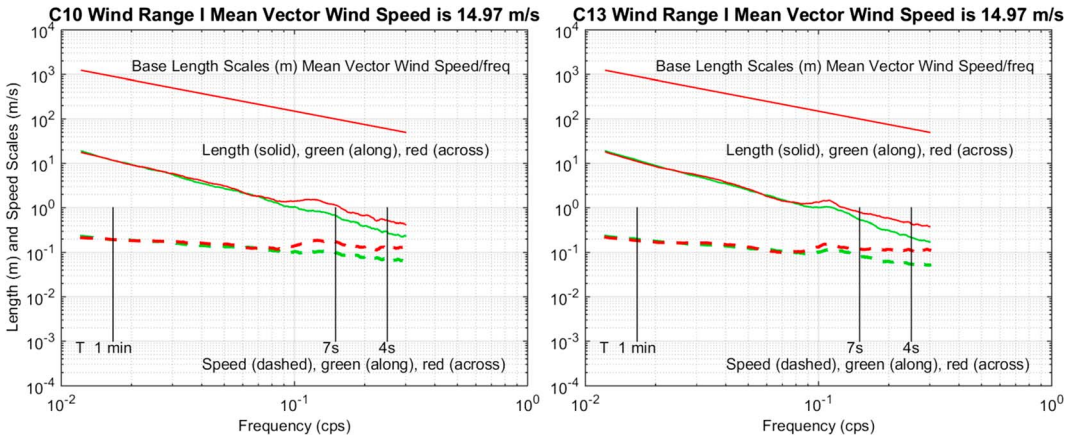

Figure 10. Intrinsic velocity and spatial scales derived from 1-s winds for C10, (left panel) and C13 (right panel) for wind range I from 0.01 to 0.3 Hz. This is a composite of 11 T_0 = 30-min subsets for C10 and 21 subsets for C13 occurring on 7 January 2014. The vertical lines denote frequencies of 1/60, 0.15, and 0.25 Hz. Spatial scales are solid, and velocity scales are dashed. DOF > 460. DOF = degree of freedom.

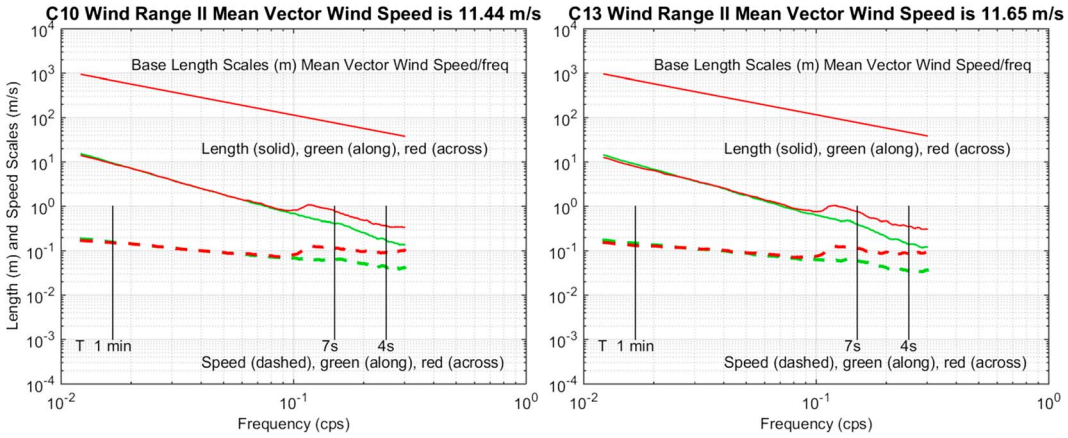

Figure 11. Intrinsic velocity and spatial scales derived from 1-s winds for C10 (left panel) and C13 (right panel) for wind range II from 0.01 to 0.3 Hz. This is a composite of 19 $T_0 = 30$-min subsets for C10 and 18 subsets for C13 occurring on 16 May 2014. The vertical lines denote frequencies of 1/60, 0.15, and 0.25 Hz. Spatial scales are solid, and velocity scales are dashed. DOF > 750. DOF = degree of freedom.

whether along or across the mean vector wind, the spatial scales are all of order 2 to 0.2 m across all the frequencies but in the range from 0.15 to 0.25 Hz, the spatial scales (Table 4) in wind ranges I and II are of order 0.2 to 0.7 m and 0.1 m in wind range III (0.19 to 0.29 Hz). In these same frequency bands, speed scales are of order 4 to 14 cm/s in wind ranges I and II and 2 to 5 cm/s in wind range III. In particular, the fidelity to the $-5/3$ power law as represented by C13 in wind range I for the frequencies in Table 4 provides turbulent spatial scales that are 33.4 ± 9.3 cm for the along component and 59.0 ± 9.9 cm for the across component with velocity scales of 6.4 ± 0.8 cm/s for the along component and 11.5 ± 0.3 cm/s for the across component.

Where these events significantly deviate from Kolmogorov's similarity hypotheses outside the narrowband between 0.15 and 0.25 Hz for the first two wind ranges and for all frequencies in wind range III, the intrinsic turbulent velocity and spatial scales are still relevant and can quantify what may be important in the energy cascade from larger to smaller eddies. The extent to which these processes may be anisotropic could highlight other components in the energy balance (Bewley et al., 2012). Other implications from these intrinsic scales might yield a means for improving our understanding of coupling at the air-sea interface (fluxes of momentum in particular) for both the atmosphere and the ocean.

The fidelity to the $-5/3$ power law is in question here, the results from C13 in wind range I notwithstanding, because from Figures 10–12 the evidence when looking at the intrinsic turbulent velocity and spatial scales

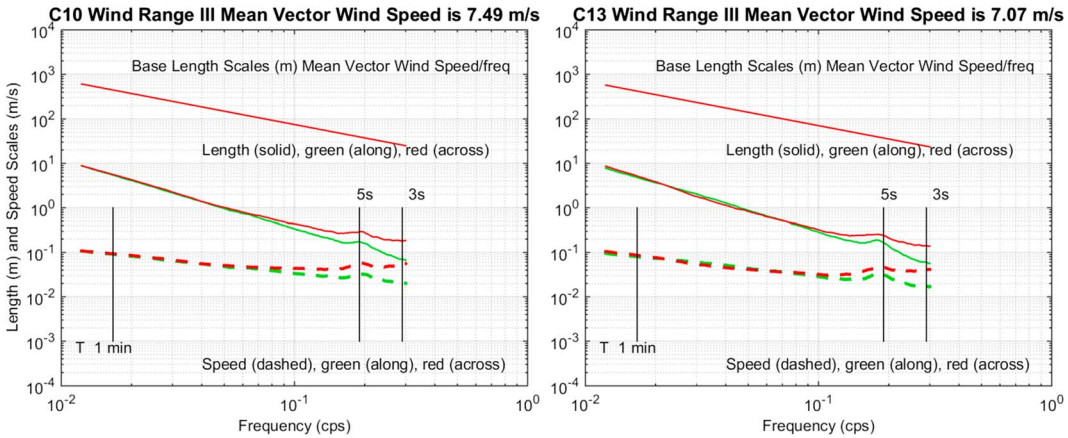

Figure 12. Intrinsic velocity and spatial scales derived from 1-s winds for C10 (left panel) and C13 (right panel) for wind range III from 0.01 to 0.3 Hz. This is a composite of 46 $T_0 = 30$-min subsets for C10 and 44 subsets for C13 occurring on 4 May 2014. The vertical lines denote frequencies of 1/60, 0.19, and 0.29 Hz. Spatial scales are solid, and velocity scales are dashed. DOF > 1,800. DOF = degree of freedom.

show anisotropy beginning near 0.09 Hz for all three wind ranges and is near the high end of the shear production range (10^{-3} to 10^{-1} Hz) from Mikkelsen et al. (2017). The manifestations of this are reflected in the statistics of the turbulent velocity and spatial scales from Table 4 where the across scales for both velocity and length are very roughly 2 times larger than those along the mean vector wind.

4. Discussion

An opportunity to look at small turbulence scales in two at-sea locations over the WFS where 1-s wind data were collected during 2013 and 2014 provides a unique window into the high frequency variability in this domain that is so important in our goal to improve the momentum flux algorithms operant in numerical models that employ coupling schemes that may not be optimal. Our ultimate goal is to improve both the model ocean circulation fields and the model atmospheric circulation fields over the WFS domain. We make no claim that this is an unprecedented data set, but there is a paucity of suitable data obtained in at-sea environments where these issues of air-sea interaction can be examined against the background of what is presently known about the transfer of momentum to the sea surface.

We suggest that $T_0 = 1{,}800$ s (30 min) is a reasonable mean vector wind time scale for the unique WFS domain in computing mean vector wind velocities and falls within the spectral gap as described by Harper et al. (2009). Moreover, this time scale also provided an ensemble of subsets for each of the events discussed here that are quasi-stationary. These subsets are essentially independent, by virtue of the independence time scales described in section 3.2 above and are akin to the flight legs described in Zhang et al. (2009). Their data were obtained from aircraft over periods of 3 min or more.

Whether or not local isotropy and Kolmogorov's similarity hypothesis can be exploited is a question that has been addressed in a limited way because of the shortcomings of our 1-s sample rate. Nevertheless, we were able to compute where the −5/3 law appears to be operant (wind range I for C13) and were able to compute the turbulent quantities: ε, u^*, τ, and C_d (the dissipation rate, the frictional velocity, the surface stress, and the drag coefficient, respectively). For the other cases where there were deviations from the −5/3 power law, we could still tease out the intrinsic turbulent velocity and spatial scales in Figures 10–12, derived directly from the one-dimensional turbulent power spectra $\phi(f)$ provided in Figures 7–9.

For the particular event in wind range I for C13, the −5/3 power law appears to be relevant. But the turbulent quantities derived therefrom (ε, u^*, τ, and C_d) yielded values considerably larger than expectations in a typical atmospheric surface layer (Högström, 1996). We compared these values with the bulk statistics for this event that consisted of 21 subsets of 1,800 s each using a variable drag coefficient (C_d) as described in Large and Pond (1981). The results yield turbulence parameters that underestimate the statistics in Table 3 by a factor of approximately 2 or more. Donelan et al. (1997) analyzed high-resolution wind data from ship observations. They found discrepancies between drag coefficients derived from dissipation estimates and those derived using the method of Large and Pond (1981) and suggest that these differences may be due to the effects of opposing swells in conditions of moderate and light winds. Wave state may also be a factor (Drennan et al., 1999). How this might impact the momentum flux algorithms in our WFS circulation models is unclear. What we take from this is that there appears to be dissipation rates and surface stresses that are larger than standard models would suggest. The larger than expected drag coefficients and fluxes in our study may be related to swells and or wave state as described above or they may be real. This can be tested in the future when collocated wave observations become available. Admittedly, the shortcomings of not having data that sample all three turbulent velocity components is something that can only be addressed with more observations using sample rates of at least 5 Hz (Harper et al., 2009).

The intrinsic turbulent velocity and spatial scales for all three wind ranges derived directly from $\phi(f)$ are summarized in Table 4 over the higher end (0.15 to 0.29 Hz) for those that are plotted in Figures 10–12. These span frequencies from 0.01 up to 0.3 Hz. The base length scales ($L_b = U_0/f$) range from 1,220 m down to 25 m for all three wind ranges. All turbulent spatial scales above 0.1 Hz are of order 1 m or less and range from 0.2 to 2 m. In particular, the fidelity to the −5/3 power law as represented by C13 in wind range I provides turbulent spatial scales that are 0.33 ± 0.09 m for the along component and 0.59 ± 0.1 m for the across component. The velocity scales are 6.4 ± 0.8 cm/s for the along component and 11.5 ± 0.3 cm/s for the across component. These values on the order of meters and centimeters are consistent with the small-eddy limit in

the inertial subrange and may apply despite evidence of anisotropy (Bewley et al., 2012; MacCready, 1962). Whether or not these scales relate to the eddies themselves is a question that remains unresolved. To this point, Mikkelsen et al. (2017) state that the smallest eddy sizes within the shear production subrange are of a size roughly on the order of the measurement height (10 m) above which isotropy cannot be assumed as these eddies sense the presence of the surface boundary, an order of magnitude larger than those in Figures 10–12. These then cascade to smaller and smaller scales down to fractions of a meter (Kolmogorov length scales). From his data over ground at 10 m the −5/3 power law appears extant for frequencies above 0.1 Hz unlike the slope for C13 in wind range I, which begins near 0.15 Hz (Figure 7). Moreover, near 0.1 Hz (Figure 10) the turbulent spatial scales are of order 1 m, an order of magnitude less than 10 m, yet here is where there appears to be evidence of anisotropy spanning frequencies from 0.09 Hz all the way to the limit of 0.3 Hz and suggests that eddy size is not a factor.

The efficacy of our analyses point to deviations from the Kolmogorov similarity hypotheses that entail assumptions of isotropy and that eddy motions in the inertial subrange may be assumed to be independent of viscosity and thus determined entirely by the rate of energy transfer which in turn is equal to the rate of energy dissipation. However, despite evidence of anisotropy from Figure 10, the −5/3 power law as represented by C13 in wind range I (Figure 7) seems to be valid from 0.15 to 0.25 Hz.

From Zhang et al. (2009), Zhang (2010), and Zhang et al. (2011), the fidelity to the −5/3 power law applies for frequencies above 0.1 Hz and isotropy appears to be valid. But these observations were obtained aloft in aircraft well above 100-m height and thus are unlikely to sense the surface boundary to the extent present in our data. Mikkelsen et al. (2017) also acknowledge the effects of the surface boundary in compromising assumptions of isotropy near the surface but also shows good agreement with the −5/3 power law.

Finally, our results point to a need for more observations particularly in sampling all three wind components where momentum flux can be computed directly. Also, the larger than expected turbulence quantities we found (Table 3) should require a closer examination of momentum flux algorithms presently operant in numerical models of ocean and atmospheric circulation fields over the WFS domain.

Acknowledgments
Coastal ocean observing within the College of Marine Science, University of South Florida was initiated in 1993 through a cooperative agreement with the U.S. Geological Survey. State of Florida support for a Coastal Ocean Monitoring and Prediction System (COMPS) was obtained in 1997. Jun Zhang was supported by NSF grants AGS1822128 and AGS1654831. Various awards were sustaining through the present time with external support now deriving from the Southeast Coastal Ocean Observing Regional Association (SECOORA) as a pass through from NOAA Grant NA16NOS0120028. We are particularly grateful for the excellent staff support provided through our Ocean Circulation Group. J. Donovan is responsible for all computer and data organization matters, and J. Law is responsible for all sea going operations. Without such excellent staff, support none of our work would be possible. The in situ wind data can be downloaded from ftp://ocgweb.marine.usf.edu/pub/Mayer_etal_2019_Surface_layer_turbulence_from_1sec_winds/.

References

Bewley, G. P., Chang, K., & Bodenschatz, E. (2012). On integral length scales in anisotropic turbulence. *Physics of Fluids*, *24*(6), 061702. https://doi.org/10.1063/1.4726077

Donelan, M. A., Drennan, W. M., & Katsaros, K. B. (1997). The air-sea momentum flux in conditions of mixed wind sea and swell. *Journal of Physical Oceanography*, *27*(10), 2087–2099. https://doi.org/10.1175/1520-0485(1997)027<2087:TASMFI>2.0.CO;2

Drennan, W. M., Kahma, K. K., & Donelan, M. A. (1999). On momentum flux and velocity spectra over waves. *Boundary-Layer Meteorology*, *92*(3), 489–515. https://doi.org/10.1023/A:1002054820455

Drennan, W. M., Taylor, P. K., & Yellland, M. J. (2005). Parameterizing the sea surface roughness. *Journal of Physical Oceanography*, *35*(5), 835–848. https://doi.org/10.1175/JPO2704.1

Dupuis, H., Taylor, P. K., Weill, A., & Katsaros, K. (1997). Inertial dissipation method applied to derive turbulent fluxes over the ocean during the Surface of the Ocean, Fluxes and Interactions with the Atmosphere/Atlantic Stratocumulus Transition Experiment (SOFIA/ASTEX) and Structure des Echanges Mer-Atmosphere, Proprietes des Heterogeneites Oceaniques: Recherche Experimentale (SEMAPHORE) experiments with low to moderate wind speeds. *Journal of Geophysical Research*, *102*, 21,115–21,129.

Edson, J. B., Fairall, C. W., Mestayer, P. G., & Larsen, S. E. (1991). A study of the inertial-dissipation method for computing air-sea fluxes. *Journal of Geophysical Research*, *96*(C6), 10,689–10,711. https://doi.org/10.1029/91JC00886

Fairall, C. W., Bradley, E. F., Rogers, D. P., Edson, J. B., & Young, G. S. (1996). Bulk parameterization of air–sea fluxes for TOGA COARE. *Journal of Geophysical Research*, *101*(C2), 3747–3764. https://doi.org/10.1029/95JC03205

Fairall, C. W., & Larsen, S. E. (1986). Inertial-dissipation methods and turbulent fluxes at the air-ocean interface. *Boundary-Layer Meteorology*, *1986*(34), 287–301.

Harper, B. A., J. D. Kepert, & J. D. Ginger (2009). Guidelines for converting between various wind averaging periods in tropical cyclone conditions. WMO, *Sixth tropical cyclone RSNCs/TCWCs technical coordination meeting*. Brisbane, Australia, 2 to 5 November, 2009.

He, R., & Weisberg, R. H. (2003). A loop current intrusion case study on the West Florida shelf. *Journal of Physical Oceanography*, *33*(2), 465–477. https://doi.org/10.1175/1520-0485(2003)033<0465:ALCICS>2.0.CO;2

Högström, U. (1996). Review of some basic characteristics of the atmospheric surface layer. *Boundary-Layer Meteorology*, *78*(3-4), 215–246. https://doi.org/10.1007/BF00120937

Kaimal, J. C., & Finnigan, J. J. (1994). *Atmospheric boundary layer flows: Their structure and measurement* (p. 289). New York: Oxford University Press.

Kaimal, J. C., Wyngaard, C., Izumi, Y., & Cote, O. R. (1972). Spectral characteristics of surface-layer turbulence. *Quarterly Journal of the Royal Meteorological Society*, *98*(417), 563–589. https://doi.org/10.1002/qj.49709841707

Katsaros, K. B., Donelan, M. A., & Drennan, W. M. (1993). Flux measurements from a SWATH ship in SWADE. *Journal of Marine Systems*, *4*(2-3), 117–132. https://doi.org/10.1016/0924-7963(93)90003-5

Kolmogrov, A. N. (1941). On dependence (decay) of isotropic turbulence in an incompressible viscous fluid. *Doklady Akademii Nauk SSSR*, *31*, 538.

Large, W. G., & Pond, S. (1981). Open ocean momentum flux measurements in moderate to strong winds. *Journal of Physical Oceanography*, *11*(3), 324–336. https://doi.org/10.1175/1520-0485(1981)011<0324:OOMFMI>2.0.CO;2

Li, Z., & Weisberg, R. H. (1999). West Florida continental shelf response to upwelling favorable wind forcing, 2: Dynamics. *Journal of Geophysical Research*, *104*(C10), 23,427–23,442. https://doi.org/10.1029/1999JC900205

Liu, Y., & Weisberg, R. H. (2012). Seasonal variability on the West Florida Shelf. *Progress in Oceanography*, *104*, 80–98. https://doi.org/10.1016/j.pocean.2012.06.001

Lumley, J. L. (1967). Similarity and turbulent energy spectrum. *Physics of fluids*, *10*(4), 855. https://doi.org/10.1063/1.1762200

MacCready, P. B. Jr. (1962). *The inertial subrange of atmospheric turbulence*. Altadena, CA: Meteorology Research, Inc.

Mayer, D. A., Weisberg, R. H., Zheng, L., & Liu, Y. (2017). Winds on the West Florida Shelf: Regional comparisons between observations and model estimates. *Journal of Geophysical Research: Oceans*, *122*, 834–846. https://doi.org/10.1002/2016JC012112

Mikkelsen, T. S., Larsen, E., Jorgensen, H. E., Astrup, P., & Larsen, X. G. (2017). Scaling of turbulence spectra measured in strong shear flow near the Earth's surface. *Physica Scripta*, *92*(12), 124002. https://doi.org/10.1088/1402-4896/aa91b2

Miyake, M., Stewart, R. W., & Burling, R. W. (1970). Spectral and cospectra of turbulence over water. *Quarterly Journal of the Royal Meteorological Society*, *96*(407), 138–143. https://doi.org/10.1002/qj.49709640714

Potter, H., Graber, H. C., Williams, N. J., Collins, C. O., Ramos, R. J., & Drennan, W. M. (2015). In situ measurements of momentum fluxes in typhoons. *Journal of the Atmospheric Sciences*, *72*(1), 104–118. https://doi.org/10.1175/JAS-D-14-0025.1

Sciremammano, F. Jr. (1979). A suggestion for the presentation of correlations and their significance levels. *Journal of Physical Oceanography*, *9*(6), 1273–1276. https://doi.org/10.1175/1520-0485(1979)009<1273:ASFTPO>2.0.CO;2

Smith, S. D. (1980). Wind stress and heat flux over the ocean in gale force winds. *Journal of Physical Oceanography*, *10*(5), 709–726. https://doi.org/10.1175/1520-0485(1980)010<0709:WSAHFO>2.0.CO;2

Sreenivasan, K. R. (1995). On the universality of the Kolmogorov constant. *Physics of Fluids*, *7*(11), 2778–2784. https://doi.org/10.1063/1.868656

Taylor, G. I. (1935). Statistical theory of turbulence I–IV. *Proceedings of Royal Society of London, Series A*, *151*, 421.

Taylor, P. K., & Yelland, M. J. (2001). The dependence of sea surface roughness on the height and steepness of the waves. *Journal of Physical Oceanography*, *31*(2), 572–590. https://doi.org/10.1175/1520-0485(2001)031<0572:TDOSSR>2.0.CO;2

Weisberg, R. H., & He, R. (2003). Local and deep-ocean forcing contributions to anomalous water properties on the West Florida Shelf. *Journal of Geophysical Research*, *108*(C6), 3184. https://doi.org/10.1029/2002JC001407

Weisberg, R. H., Liu, Y., & Mayer, D. A. (2009). West Florida Shelf mean circulation observed with long-term moorings. *Geophysical Research Letters*, *36*, L19610. https://doi.org/10.1029//2009GL040028

Yelland, M. J., Moat, B. I., Taylor, P. K., Pascal, R. W., Hutchings, J., & Cornell, V. C. (1998). Measurements of the open ocean drag coefficient corrected for air flow disturbance by the ship. *Journal of Physical Oceanography*, *28*(7), 1511–1526. https://doi.org/10.1175/1520-0485(1998)028<1511:WSMFTO>2.0.CO;2

Yelland, M. J., & Taylor, P. K. (1996). Wind stress measurements from the open ocean. *Journal of Physical Oceanography*, *26*(4), 541–558. https://doi.org/10.1175/1520-0485(1996)026<0541:WSMFTO>2.0.CO;2

Yelland, M. J., Taylor, P. K., Consterdine, I. E., & Smith, M. H. (1994). The use of the inertial dissipation technique for shipboard wind stress determination. *Journal of Atmospheric and Oceanic Technology*, *11*(4), 1093–1108. https://doi.org/10.1175/1520-0426(1994)011<1093:TUOTID>2.0.CO;2

Yu, B., Chowdhury, A. G., & Masters, F. J. (2008). Hurricane wind power spectra, cospectra and integral length scales. *Boundary-Layer Meteorology*, *129*(3), 411–430. https://doi.org/10.1007/s10546-008-9316-8

Zhang, J. A. (2010). Estimation of dissipative heating using low-level in situ aircraft observations in the hurricane boundary layer. *Journal of the Atmospheric Sciences*, *67*(6), 1853–1862. https://doi.org/10.1175/2010JAS3397.1

Zhang, J. A., Drennan, W. M., Black, P. G., & French, J. R. (2009). Turbulence structure of the hurricane boundary layer between the outer rainbands. *Journal of the Atmospheric Sciences*, *66*(8), 2455–2467. https://doi.org/10.1175/2009JAS2954.1

Zhang, J. A., Marks, F. D., Montgomery, M. T., & Lorsolo, S. (2011). An estimation of turbulent characteristics in the low-level region of intense hurricanes Allen (1980) and Hugo (1989). *Monthly Weather Review*, *139*(5), 1447–1462. https://doi.org/10.1175/2010MWR3435.1